LETTER

Postsynthetic Metalation of a New Metal−Organic Framework To Improve Methane Working Storage Capacity

Ha L. Nguyen,* Roc Matheu, Christian S. Diercks, Tan L. H. Doan, Binh T. Nguyen, and Kyle E. Cordova

Read Online

ACCESS | Metrics & More | Article Recommendations | SI Supporting Information

ABSTRACT: In the design of metal−organic frameworks (MOFs) for methane storage, a balance must be struck between the porosity of the MOF, the internal pore environment, the adsorption thermodynamics, and the density. Herein, we report the design of a new Zr-MOF, termed MOF-700, which was metalated with various Cu(II) salts to produce an isoreticular series of three new, highly porous MOFs (MOF-701, MOF-702, and MOF-703). The position of the metalated sites was determined by X-ray absorption spectroscopy, and the metalated frameworks were found to display high volumetric methane storage working capacities [206 cm^3(STP) cm^{-3} at 298 K and 5.0−80.0 bar for MOF-701]. This constitutes an improvement of 50% over the performance of the parent MOF-700 [137 cm^3(STP) cm^{-3}] and highlights the prospect of optimization of methane working storage capacity by postsynthetic metalation.

Metal−organic frameworks (MOFs) have emerged as viable candidates for the storage of methane.[1−3] Over the past 20 years, many MOFs have been reported where the following concepts were implemented toward increasing the working storage capacity of methane: (i) the isoreticular principle;[4] (ii) increasing the packing density of adsorbed methane;[5,6] (iii) introducing framework flexibility and dynamism;[7] and (iv) fine-tuning of pore geometry and size to maximize methane−framework and methane−methane interactions.[8−11] Here, we introduce a new tool to achieve high methane working capacities, which consists of introducing coordinatively saturated metals that only enhance methane−framework interactions at high pressure. Specifically, the postsynthetic metalation (PSM)[12] of a new Zr-based MOF with Cu(II) salts increases the methane uptake at high pressures while it decreases the uptake at low pressures, which results in a net improvement of volumetric methane storage working capacity. In particular, the MOF metalated with Cu(NO$_3$)$_2$ (MOF-701) achieves a high volumetric methane storage working capacity of 206 cm^3(STP) cm^{-3} at 298 K and 5.0−80 bar, which is among the highest values reported for methane storage by porous materials.

Microcrystalline powder of MOF-700 was solvothermally synthesized at 120 °C for 3 days (see Sections S1 and S2 in the Supporting Information). Structural solution of this new

material was performed using powder X-ray diffraction (PXRD) techniques, because the low resolution of single-crystal data only allowed the determination of the positions of the Zr-oxo cluster. As it was expected that MOF-700 adopts a face-centered cubic (**fcu**) topology arising from linking 12-c cuboctahedral-shaped Zr$_6$O$_4$(OH)$_4$(−CO$_2$)$_{12}$ secondary building units (SBUs) with 2-c linear organic linkers (4,4′-[oxalylbis(imino)]bis(2-hydroxybenzoic acid), H$_4$−ODA) (Figure 1),[12] a structural model was generated and Rietveld refinement was performed against the experimental PXRD pattern leading to optimized unit-cell parameters (F23, a = 32.1520(4) Å), atomic positions, and converging R factors (R$_p$ = 6.16%, R$_{wp}$ = 8.20%) (see Figure 2d, presented later in this work, as well as Section S3 in the Supporting Information). The three-dimensional (3D) crystal structure (Figure 1a) exhibited the triangular pore apertures that open to one large

Figure 1. Crystal structure of MOF-700 adopting two types of pore as a result of its *fcu* topology. (a) Bimetallic cluster after postsynthetic metalation leading to square pyramidal coordination of Cu(II) complex. (b) k^2-weighted Cu-extended X-ray absorption fine structure (Cu-EXAFS) spectra for MOF-702 (black) and best fit (red line) in (c) *k*-space and (d) R-space. Fit range: $3 < k < 11$ Å^{-1}; $1 < R < 4.0$ Å. Fit window: Hanning. Atom colors: Zr, blue; C, gray; O, red; N, green; Cu, orange. All H atoms are omitted for clarity.

octahedral cage (~23 Å) and one small tetrahedral cage (8.5 Å).

We then sought to perform PSM of MOF-700 using various Cu(II) salts with the hypothesis that the metal complex sites would be bound to Zr-oxo cluster through direct oxo (μ_3-O) binding.[13] Note that introducing metal complexes onto the structure of MOF is an advantageous strategy for (i) imparting strong binding sites within the internal pore environment for guest molecules to interact with without sacrificing overall porosity; (ii) increasing the crystal density to enhance volumetric capacity of stored gases; and (iii) optimizing pore shape, size, and volume. As such, MOF-700 was subjected to PSM with CuX$_2$ (where X = NO$_3$, OAc, or Cl) by directly immersing the parent MOF-700 in a dimethylformamide (DMF) solution containing the respective Cu(II) salt [Cu(NO$_3$)$_2$, MOF-701; Cu(OAc)$_2$, MOF-702; CuCl$_2$, MOF-703] (see Section S2). During the metalation process, a noticeable color change in the MOF-700 solid (from beige to green) was clearly observed, which is consistent with previous reports for similar metalation processes (see Section S2).[14]

After the metalation process was completed, MOF-701, MOF-702, and MOF-703 were washed thoroughly and activated to ensure that any unbound or unreacted Cu salts were removed from the pores. Cu and Zr elemental distribution mapping by energy-dispersive X-ray spectroscopy demonstrated that Cu was highly disperse throughout entire crystallites of each metalated MOF (see Figures 2b and 2c, presented later in this work, as well as Section S7 in the Supporting Information). As an initial assessment of the nature of the complexation, Raman spectroscopy was employed.
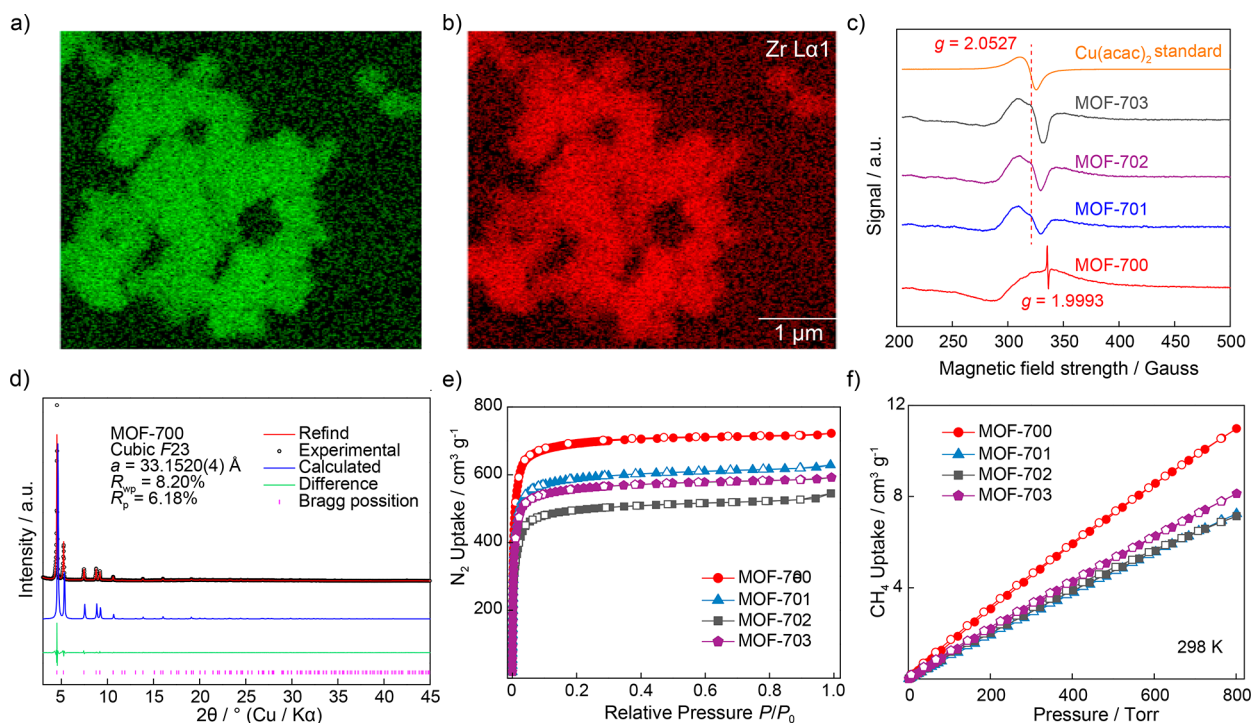
Figure 2. (a, b) Elemental mapping via energy-dispersive X-ray spectroscopy of MOF-702 displays highly disperse Zr and Cu throughout the bulk crystallites. (c) Electron paramagnetic resonance (EPR) spectroscopy confirmed the oxidation state of the newly installed Cu(II) complex. The spectra of metalated MOF-701 (blue), MOF-702 (purple), and MOF-703 (black) display characteristic features of d_9 Cu(II) as proven by comparison to the model compound, Cu(acac)$_2$ (orange). (d) Representative Rietveld refinement of MOF-700 yields converging *R* factors. (e) N$_2$ adsorption isotherms of MOF-700 (red) at 77 K, compared to the metalated analogues: MOF-701 (blue), MOF-702 (black), and MOF-703 (purple). (f) Low-pressure CH$_4$ adsorption isotherms at 298 K for MOF-700 (red), MOF-701 (blue), MOF-702 (black), and MOF-703 (purple). Open and closed symbols represent the adsorption and desorption branches, respectively.

Functioning as a control, the parent MOF-700 demonstrated no specific Raman shift whereas MOF-701, MOF-702, and MOF-703 all exhibited new Raman vibrational bands due to Cu(II) complexation. Specifically, pronounced vibrational bands for Cu−O were observed in the 200 to 400 cm^{-1} regions (Section S4 in the Supporting Information).[15] Electron paramagnetic resonance (EPR) spectroscopy was then applied to all members of the series in order to confirm the oxidation state of the newly installed Cu(II) complex. Indeed, the resulting spectra display characteristic features of a d^9 Cu(II) complex with g-factors of ∼2.0527 for MOF-701, MOF-702, and MOF-703 (see Figure 2a, as well as Section S5 in the Supporting Information). When comparing to a model compound, namely Cu(acac)$_2$, these values are in satisfactory agreement for the divalent state of a Cu-based complex.[16] It is important to note that the parent MOF-700 displayed a g-factor of 1.993, which is distinctly different from its metalated analogues, thus ruling out the possibility of unreacted starting materials immobilized within the pores.

Cu K-edge X-ray absorption spectroscopy (XAS) was then performed for MOF-701, MOF-702, and MOF-703 to elucidate the coordination environment of the Cu(II) centers within each respective MOF. X-ray absorption near-edge structure (XANES) spectra of MOF-701, MOF-702, and MOF-703 produced identical spectra as noted by an intense white line at ∼8998 eV,[13] consistent with a Cu(II) oxidation state. The analogous XANES spectra displayed by MOF-701, MOF-702, and MOF-703 indicates that the oxidation state and first coordination sphere of Cu(II) complexes in each of these metalated MOFs are identical (Section S7 in the Supporting Information). After these results, MOF-702 was chosen, as a representative example, to be studied by extended X-ray absorption fine structure (EXAFS) in order to elucidate the coordination environment of the Cu(II) in detail. The Cu EXAFS fitting results of MOF-702 demonstrated that the Cu central complex site was surrounded by 4 O atoms with Cu−O bond lengths of 1.95 ± 0.01 Å in the first shell, 1 C/O atom in the second shell with a bond length of 2.33 ± 0.04 Å, and 3 Zr atoms in the third shell which Cu−Zr bond lengths of 3.62 ± 0.05 Å (see Figures 1c and 1d, as well as Section S7). The results are in good agreement with the fact that the Cu(II) complex sites are located near the Zr-oxo cluster via direct μ_3-O binding (Figure 1b). In addition, the Cu(II) atom binds to 3 water moieties, and one oxygen from carboxylate-based linker in a square pyramidal geometry (Figure 1b). For satisfying charge balance, the respective counteranions used for each Cu(II) salt were located within the pores similar to previous reports in the isostructural UiO-68 material.[17] The coordination of the Cu(II) atoms to the Zr-oxo cluster was further confirmed by comparing the Fourier transform infrared (FTIR) spectroscopy of the parent MOF-700 with that of the metalated MOFs. We found that the FTIR spectrum of MOF-700 is coincident with the FTIR spectra of the metalated MOFs. This clearly rules out coordination of Cu(II) to the amide functionality in the linker as Cu(II)-amide would result in a difference in FTIR spectra (Section S6 in the Supporting Information).

With the nature of the complexation elucidated, attention was then placed on quantifying the degree of metalation. Upon digesting the metalated MOFs, inductively coupled plasma−optical emission spectrometry analysis revealed loadings of 11.17 wt % [Cu(NO$_3$)$_2$], 12.08 wt % [Cu(OAc)$_2$], and 11.89 wt % [CuCl$_2$] for MOF-701, MOF-702, and MOF-703,

respectively (see Section S2). When considering the degree of loading as a function of complex site per metal cluster, MOF-701, MOF-702, and MOF-703 were calculated to be quantitative (100%).

As demonstrated by PXRD analysis, the crystallinity of MOF-700 was retained over the course of the postsynthetic metalation procedures (see Section S3). With knowledge of the degree of Cu(II) metalation, computational models of metalated MOF-700 were generated with the appropriate Cu(II) occupancies. The symmetry of metalated MOFs was reduced to P23, which is a Klassengleiche subgroup of F23 (see Section S3). From the N$_2$ isotherms at 77 K, the Brunauer−Emmett−Teller (BET) surface areas were calculated to be 2350, 1950, and 2300 m^2 g^{-1} for MOF-701, MOF-702, and MOF-703, respectively, which are all less than the BET surface area calculated for MOF-700 (2900 m^2 g^{-1}) (Figure 2e). The presence of the anions within the internal pore environment of the metalated MOFs reduces the size of the octahedral cage from 23 Å in MOF-700 to 16.5, 17.0, and 18.5 Å for MOF-701, MOF-702, and MOF-703, respectively, based on the pore size distribution analysis obtained from nonlocal density functional theory (DFT) calculations (Section S9).

Regardless of metalation, MOF-701, MOF-702, and MOF-703 still retain high surface areas and pore volumes (0.97, 0.82, and 0.92 cm^3 g^{-1} for MOF-701, MOF-702, and MOF-703, respectively).

We estimated the crystal densities of MOF-701, MOF-702, and MOF-703 from their structural formulas.[18] We also compared the crystal density values to the experimental densities calculated from the measured pore volume (V_p) obtained from the N$_2$ isotherms at 77 K and the measured skeletal densities (ρ_{sk}) obtained from a He free space measurement at 298 K (Sections S10 and S11).[11] The crystal density values of MOF-701, MOF-702, and MOF-703 were 9.9%, 22.2%, and 7.5% lower than those obtained experimentally (Table S8 in the Supporting Information). We used the densities estimated from the crystal density formulas[18] to further calculate the methane uptake at high pressure as it represents an underestimation of the real value. In addition, we provide the tap density of the MOF series for consideration of future practical applications (see Table S8).

An outstanding challenge in the design of adsorbent materials for high volumetric methane working capacity is balancing the interplay between surface area, optimized pore environment, thermodynamics of adsorption, and crystal density.[19,24] When considering that postsynthetic metalation of MOF-700 led to materials that retained a high surface area yet reduced their pore sizes and increased their total density, we sought to assess the methane adsorption properties of these materials. As such, low-pressure (1.0 bar) methane isotherms were collected at 278, 288, and 298 K (Figure 2f, Section S10 in the Supporting Information). The isosteric heat of adsorption (Q_{st}) was then calculated by applying a virial-type expansion equation.[10] For MOF-700, the Q_{st} value was calculated to be 13.4 kJ mol^{-1}, which, as expected, was lower than those calculated for MOF-701, MOF-702, and MOF-703 (14.7, 18.6, and 14.2 kJ mol^{-1}, respectively) (recall Section S10). Although the values for the metalated members increased due to higher interactions of methane with the framework and the fact that they possessed smaller pores when compared to the parent structure, they remain moderate when compared to MOFs containing open metal sites.[21] Indeed, the

Q_{st} values of the metalated MOFs are in the ideal range when considering the usability of all adsorbed methane under the prescribed working conditions.[10]

High-pressure methane adsorption isotherms (up to 80 bar) were then collected at 298 K (see Table 1, as well as Section

Table 1. Comparison of Methane Storage Capacities for Relevant High Performing MOFs at 35, 65, and 80 bar and 298 K

MOF	Total Uptake [cm³(STP) cm⁻³]			Working Capacity[a] [cm³(STP) cm⁻³]			ref
	at 35 bar	at 65 bar	at 80 bar	at 35 bar	at 65 bar	at 80 bar	
MOF-700	103	147	163	77	120	137	this work
MOF-701	150	212	236	120	182	206	this work
MOF-702	122	175	195	94	147	167	this work
MOF-703	128	181	205	104	157	181	this work
LIFM-82	196	245	271	143	182	218	10
MOF-905	145	207	228	120	175	203	11
HKUST-1	225	251	271	153	190	200	11
MAF-38	225	263	275	147	187	197	6
$_{mono}$UiO-66_D	140	211	245	90	172	195	19
MOF-177	122	176	205	102	156	188	11
ST-2	112	175	200	99	155	187	20
PCN-14	200	230	250	128	157	178	21
UTSA-76a	211	257	n/a	151	197	n/a	22
UTSA-110a	175	240	n/a	125	190	n/a	22
Co(bdp)	161	203	n/a	155	197	n/a[b]	18
X-dia-1-Ni	150	189	n/a	110	149	n/a	23

[a]Calculated at 5.0−35, 5.0−65, and 5.0−80 bar. [b]Calculated at 5.8−35, 5.8−65 bar.

S11 in the Supporting Information). The excess methane isotherms are presented in Figures S26, S28, and S30 in the Supporting Information. As shown in Table 1 and Figure 3a, metalated MOF-701, MOF-702, and MOF-703 exhibit significantly higher total volumetric methane uptake capacities than the parent MOF-700. The profile of the isotherms clearly indicates that, at low pressures (0−10 bar), the inorganic SBU
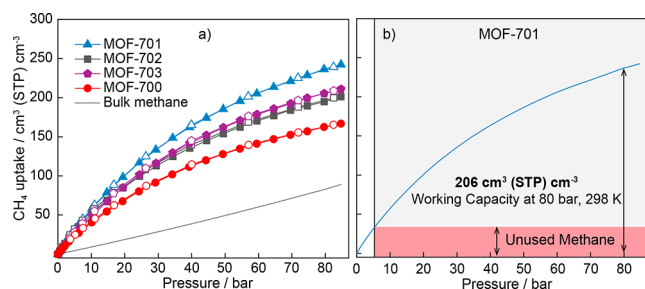
Figure 3. (a) Total methane isotherms at 298 K for MOF-700 (red), MOF-701 (blue), MOF-702 (black), and MOF-703 (purple). Open and closed symbols represent the adsorption and desorption branches, respectively. The bulk density of methane is represented by the black dashed curve for comparison. (b) Working capacity of MOF-701 under the prescribed practical operating conditions (298 K and 5.0−80 bar).

is the primary contributor to gas adsorption (Figure 3a). The difference in total uptake capacities is stark at 35 bar and increasingly diverge upon reaching pressures of 80 bar (see Table 1 and Figure 3). Specifically, the total methane uptake capacities of MOF-701, MOF-702, and MOF-703 reach 236, 195, and 205 cm³(STP) cm⁻³ at 80 bar, respectively as compared to 163 cm³(STP) cm⁻³ for MOF-700 at 80 bar (Table 1), which clearly highlights our strategy of using PSM to volumetrically improve the methane uptake capacity.

This series of MOFs exhibited moderate methane uptake capacity in the low-pressure range (0−5.0 bar), which should be advantageous in achieving larger working capacities when compared to other high-performing adsorbent materials. This observation is critical as the practicality of applying these materials for use as methane adsorbents in vehicles relies heavily on how high the volumetric working capacities can reach (desorption pressure = 5.0 bar). Indeed, MOF-701, MOF-702, and MOF-703 displayed exceptionally high methane uptake working capacities of 206, 167, and 181 cm³(STP) cm⁻³, respectively, at 298 K and 5.0−80 bar. Apart from specific pore structure, high surface area, MOF-701 with the highest density showed higher uptake than MOF-702 and MOF-703. MOF-702 possessed a lower surface area than that of MOF-701 and MOF-703, resulting in a smaller total uptake capacity of methane. Regarding the standard practice of conforming to DOE guidelines[25] with storage pressure at 65 bar, MOF-700 displayed a deliverable capacity of 120 cm³(STP) cm⁻³. MOF-701, MOF-702, and MOF-703 out-performed the pristine MOF-700, with working capacities of 182, 147, and 157 cm³(STP) cm⁻³, respectively. These values are among the best materials for methane uptake at 65 bar (Table 1). We choose MOF-701 to perform the cycling experiments. MOF-701's recycling performance was conducted for 3 consecutive cycles exhibiting negligible changes in uptake (Section S10).

PSM changes the pore size and potentially introduces new binding sites for methane. Pore size tailoring has been identified as the critical factor for methane uptake at high pressure. In contrast, Cu-methane interactions only result in an increase of methane uptake in the presence of open-metal sites.[26] Hence, our PSM tailoring strategy is restricted to metals that coordinate to the highly connected Zr clusters and do not generate open metal sites under solvent removal. It is our belief that the counteranions contribute to increasing methane uptake at high pressure.[27,28] Particularly, we anticipate that anions help create specific pockets in the MOF pores that facilitate methane sorption at high pressure. In addition, the localized charge around these anions is critical to the interaction between methane molecules and the MOF, which helps increase the packing of methane at high pressure in the case of our metalated MOF-700 series, in general, and MOF-701, in specific. In addition, the PSM of UiO-66-type MOFs has recently been explored for catalysis applications.[13] Our strategy to increase the total working capacity of methane through PSM might be applicable to highly connected Zr_6O_8 clusters that possess adequate pore sizes and volumes.[29] We envision that our strategy may be further exploited to benefit gravimetric gas uptake.

We report the syntheses and fully characterizations of a new Zr-based MOF (MOF-700) and three metalated MOFs with various Cu(II) complexes (MOF-701, MOF-702, and MOF-703). Those metalated MOFs were found to be promising candidates for methane uptake at 80 bar and 298 K. The

importance of the postsynthetic metalation strategy in methane storage at high pressure is highlighted by the fact that the methane uptake working capacity of the parent MOF-700 only reached 137 cm^3(STP) cm^{-3} while MOF-701, MOF-702, and MOF-703 displayed high methane uptake working capacities of 206, 167, and 181 cm^3(STP) cm^{-3}, respectively. It is important to note that these findings are among the highest values reported for any adsorbent material to date.[30,31]

ASSOCIATED CONTENT

ⓈⒾ Supporting Information

The Supporting Information is available free of charge at https://pubs.acs.org/doi/10.1021/acsmaterialslett.2c00597.

Synthesis, full characterizations, and gas sorption data of MOF-700, MOF-701, MOF-702, and MOF-703 (PDF)

AUTHOR INFORMATION

Corresponding Author

Ha L. Nguyen − Center for Innovative Materials and Architectures (INOMAR), Vietnam National University— Hochiminh, Hochiminh City 721337, Vietnam; Present Address: Department of Chemistry, University of California—Berkeley, Berkeley, CA 94720, USA; ⓞ orcid.org/0000-0002-4977-925X; Email: nguyen.lh@ berkeley.edu, nlha@inomar.edu.vn

Authors

Roc Matheu − Department of Chemistry, University of California—Berkeley, Berkeley, California 94720, United States; ⓞ orcid.org/0000-0001-8601-5219

Christian S. Diercks − Department of Chemistry, University of California—Berkeley, Berkeley, California 94720, United States; ⓞ orcid.org/0000-0002-7813-0302

Tan L. H. Doan − Center for Innovative Materials and Architectures (INOMAR), Vietnam National University— Hochiminh, Hochiminh City 721337, Vietnam

Binh T. Nguyen − Center for Innovative Materials and Architectures (INOMAR), Vietnam National University— Hochiminh, Hochiminh City 721337, Vietnam; Present Address: Department of Chemistry, Ho Chi Minh City of Education, Ho Chi Minh City 721337, Vietnam

Kyle E. Cordova − Materials Discovery Research Unit, Advanced Research Centre, Royal Scientific Society, Amman 11941, Jordan; ⓞ orcid.org/0000-0002-4988-0497

Complete contact information is available at:
https://pubs.acs.org/10.1021/acsmaterialslett.2c00597

Author Contributions

The manuscript was written through contributions of all authors.

Notes

The authors declare no competing financial interest.

ABBREVIATIONS

MOFs, metal−organic frameworks; PSM, postsynthetic metal-ation; STP, standard temperature and pressure; PXRD, powder X-ray diffraction; SBUs, secondary building units; XAS, X-ray absorption spectroscopy; XANES, X-ray absorption near-edge structure; EXAFS, extended X-ray absorption fine structure

REFERENCES

(1) Yaghi, O. M.; Kalmutzki, M. J.; Diercks, C. S. *Introduction to Reticular Chemistry: Metal-Organic Frameworks and Covalent Organic Frameworks*; Wiley-VCH: Weinheim, Germany, 2019; p 509.

(2) Kondo, M.; Yoshitomi, T.; Matsuzaka, H.; Kitagawa, S.; Seki, K. Three-Dimensional Framework with Channeling Cavities for Small Molecules: {[M$_2$(4, 4′-Bpy)$_3$(NO$_3$)$_4$]·xH$_2$O}$_n$ (M = Co, Ni, Zn). *Angew. Chem., Int. Ed.* **1997**, *36*, 1725−1727.

(3) He, Y.; Chen, F.; Li, B.; Qian, G.; Zhou, W.; Chen, B. Porous Metal−Organic Frameworks for Fuel Storage. *Coord. Chem. Rev.* **2018**, *373*, 167−198.

(4) Eddaoudi, M.; Kim, J.; Rosi, N.; Vodak, D.; Wachter, J.; O'Keeffe, M.; Yaghi, O. M. Systematic Design of Pore Size and Functionality in Isoreticular MOFs and Their Application in Methane Storage. *Science* **2002**, *295*, 469−472.

(5) Guo, Z.; Wu, H.; Srinivas, G.; Zhou, Y.; Xiang, S.; Chen, Z.; Yang, Y.; Zhou, W.; O'Keeffe, M.; Chen, B. A Metal-Organic Framework with Optimized Open Metal Sites and Pore Spaces for High Methane Storage at Room Temperature. *Angew. Chem., Int. Ed.* **2011**, *50*, 3178−3181.

(6) Lin, J.-M.; He, C.-T.; Liu, Y.; Liao, P.-Q.; Zhou, D.-D.; Zhang, J.-P.; Chen, X.-M. A Metal-Organic Framework with a Pore Size/Shape Suitable for Strong Binding and Close Packing of Methane. *Angew. Chem., Int. Ed.* **2016**, *55*, 4674−4678.

(7) Li, B.; Wen, H.-M.; Wang, H.; Wu, H.; Tyagi, M.; Yildirim, T.; Zhou, W.; Chen, B. A Porous Metal−Organic Framework with Dynamic Pyrimidine Groups Exhibiting Record High Methane Storage Working Capacity. *J. Am. Chem. Soc.* **2014**, *136*, 6207−6210.

(8) Zhang, M.; Zhou, W.; Pham, T.; Forrest, K. A.; Liu, W.; He, Y.; Wu, H.; Yildirim, T.; Chen, B.; Space, B.; Pan, Y.; Zaworotko, M. J.; Bai, J. Fine Tuning of MOF-505 Analogues To Reduce Low-Pressure Methane Uptake and Enhance Methane Working Capacity. *Angew. Chem., Int. Ed.* **2017**, *56*, 11426−11430.

(9) Yan, Y.; Kolokolov, D. I.; da Silva, I.; Stepanov, A. G.; Blake, A. J.; Dailly, A.; Manuel, P.; Tang, C. C.; Yang, S.; Schröder, M. Porous Metal−Organic Polyhedral Frameworks with Optimal Molecular Dynamics and Pore Geometry for Methane Storage. *J. Am. Chem. Soc.* **2017**, *139*, 13349−13360.

(10) Chen, C.-X.; Wei, Z.-W.; Jiang, J.-J.; Zheng, S.-P.; Wang, H.-P.; Qiu, Q.-F.; Cao, C.-C.; Fenske, D.; Su, C.-Y. Dynamic Spacer Installation for Multirole Metal−Organic Frameworks: A New Direction toward Multifunctional MOFs Achieving Ultrahigh Methane Storage Working Capacity. *J. Am. Chem. Soc.* **2017**, *139*, 6034−6037.

(11) Jiang, J.; Furukawa, H.; Zhang, Y.-B.; Yaghi, O. M. High Methane Storage Working Capacity in Metal−Organic Frameworks with Acrylate Links. *J. Am. Chem. Soc.* **2016**, *138*, 10244−10251.

(12) Assen, A. H.; Adil, K.; Cordova, K. E.; Belmabkhout, Y. The Chemistry of Metal-Organic Frameworks with Face-Centered Cubic Topology. *Coord. Chem. Rev.* **2022**, *468*, 214644.

(13) Abdel-Mageed, A. M.; Rungtaweevoranit, B.; Parlinska-Wojtan, M.; Pei, X.; Yaghi, O. M.; Behm, R. J. Highly Active and Stable Single-Atom Cu Catalysts Supported by a Metal−Organic Framework. *J. Am. Chem. Soc.* **2019**, *141*, 5201−5210.

(14) Manna, K.; Zhang, T.; Lin, W. Postsynthetic Metalation of Bipyridyl-Containing Metal−Organic Frameworks for Highly Efficient Catalytic Organic Transformations. *J. Am. Chem. Soc.* **2014**, *136*, 6566−6569.

(15) Tan, K.; Nijem, N.; Canepa, P.; Gong, Q.; Li, J.; Thonhauser, T.; Chabal, Y. J. Stability and Hydrolyzation of Metal Organic Frameworks with Paddle-Wheel SBUs upon Hydration. *Chem. Mater.* **2012**, *24*, 3153−3167.

(16) Godiksen, A.; Stappen, F. N.; Vennestrøm, P. N. R.; Giordanino, F.; Rasmussen, S. B.; Lundegaard, L. F.; Mossin, S. Coordination Environment of Copper Sites in Cu-CHA Zeolite Investigated by Electron Paramagnetic Resonance. *J. Phys. Chem. C* **2014**, *118*, 23126−23138.

(17) Manna, K.; Ji, P.; Lin, Z.; Greene, F. X.; Urban, A.; Thacker, N. C.; Lin, W. Chemoselective Single-Site Earth-Abundant Metal Catalysts at Metal−Organic Framework Nodes. *Nat. Commun.* **2016**, *7*, 12610.

(18) Mason, J. A.; Oktawiec, J.; Taylor, M. K.; Hudson, M. R.; Rodriguez, J.; Bachman, J. E.; Gonzalez, M. I.; Cervellino, A.; Guagliardi, A.; Brown, C. M.; Llewellyn, P. L.; Masciocchi, N.; Long, J. R. Methane Storage in Flexible Metal−Organic Frameworks with Intrinsic Thermal Management. *Nature* **2015**, *527*, 357−361.

(19) Connolly, B. M.; Aragones-Anglada, M.; Gandara-Loe, J.; Danaf, N. A.; Lamb, D. C.; Mehta, J. P.; Vulpe, D.; Wuttke, S.; Silvestre-Albero, J.; Moghadam, P. Z.; Wheatley, A. E. H.; Fairen-Jimenez, D. Tuning Porosity in Macroscopic Monolithic Metal-Organic Frameworks for Exceptional Natural Gas Storage. *Nat. Commun.* **2019**, *10*, 2345.

(20) Liang, C.-C.; Shi, Z.-L.; He, C.-T.; Tan, J.; Zhou, H.-D.; Zhou, H.-L.; Lee, Y.; Zhang, Y.-B. Engineering of Pore Geometry for Ultrahigh Capacity Methane Storage in Mesoporous Metal−Organic Frameworks. *J. Am. Chem. Soc.* **2017**, *139*, 13300−13303.

(21) Mason, J. A.; Veenstra, M.; Long, J. R. Evaluating Metal−Organic Frameworks for Natural Gas Storage. *Chem. Sci.* **2014**, *5*, 32−51.

(22) Wen, H.-M.; Li, B.; Li, L.; Lin, R.-B.; Zhou, W.; Qian, G.; Chen, B. A Metal-Organic Framework with Optimized Porosity and Functional Sites for High Gravimetric and Volumetric Methane Storage Working Capacities. *Adv. Mater.* **2018**, *30*, 1704792.

(23) Yang, Q.; Lama, P.; Sen, S.; Lusi, M.; Chen, K.; Gao, W.; Shivanna, M.; Pham, T.; Hosono, N.; Kusaka, S.; Perry, J. J., IV; Ma, S.; Space, B.; Barbour, L. J.; Kitagawa, S.; Zaworotko, M. J. Reversible Switching between Highly Porous and Nonporous Phases of an Interpenetrated Diamondoid Coordination Network That Exhibits Gate-Opening at Methane Storage Pressures. *Angew. Chem., Int. Ed.* **2018**, *57*, 5684−5689.

(24) Tian, T.; Zeng, Z.; Vulpe, D.; Casco, M. E.; Divitini, G.; Midgley, P. A.; Silvestre-Albero, J.; Tan, J.-C.; Moghadam, P. Z.; Fairen-Jimenez, D. A Sol−Gel Monolithic Metal−Organic Framework with Enhanced Methane Uptake. *Nat. Mater.* **2018**, *17*, 174−179.

(25) *Methane Opportunities for Vehicular Energy*, Advanced Research Project Agency−Energy, U.S. Dept. of Energy, Funding Opportunity No. DE-FOA-0000672, 2012.

(26) Hulvey, Z.; Vlaisavljevich, B.; Mason, J. A.; Tsivion, E.; Dougherty, T. P.; Bloch, E. D.; Head-Gordon, M.; Smit, B.; Long, J. R.; Brown, C. M. Critical Factors Driving the High Volumetric Uptake of Methane in $Cu_3(Btc)_2$. *J. Am. Chem. Soc.* **2015**, *137*, 10816−10825.

(27) Verma, G.; Kumar, S.; Vardhan, H.; Ren, J.; Niu, Z.; Pham, T.; Wojtas, L.; Butikofer, S.; Echeverria Garcia, J. C.; Chen, Y.-S.; Space, B.; Ma, S. A Robust Soc-MOF Platform Exhibiting High Gravimetric Uptake and Volumetric Deliverable Capacity for on-Board Methane Storage. *Nano Res.* **2021**, *14*, 512−517.

(28) Ubaid, S.; Assen, A. H.; Alezi, D.; Cairns, A.; Eddaoudi, M.; Belmabkhout, Y. Evaluating the High-Pressure Volumetric CH_4, H_2, and CO_2 Storage Properties of Denser-Version Isostructural Soc-Metal−Organic Frameworks. *J. Chem. Eng. Data* **2022**, *67*, 1732−1742.

(29) Bai, Y.; Dou, Y.; Xie, L.-H.; Rutledge, W.; Li, J.-R.; Zhou, H.-C. Zr-Based Metal−Organic Frameworks: Design, Synthesis, Structure, and Applications. *Chem. Soc. Rev.* **2016**, *45*, 2327−2367.

(30) Tan, J.; Tao, Y.; Zhang, X.; Wang, Q.; Zeng, T.; Shi, Z.; Cordova, K. E.; Lee, Y.; Liu, H.; Zhang, Y.-B. Control over Interpenetration for Boosting Methane Storage Capacity in Metal−Organic Frameworks. *J. Mater. Chem. A* **2021**, *9*, 24857−24862.

(31) Chen, J.-R.; Luo, Y.-Q.; He, S.; Zhou, H.-L.; Huang, X.-C. Ligand Tailoring Strategy of a Metal−Organic Framework for Optimizing Methane Storage Working Capacities. *Inorg. Chem.* **2022**, *61*, 10417−10424.